Proceedings of NCFMFP2006
2006 33rd National and 3rd International Conference on Fluid Mechanics and Fluid Power
December 7-9, 2006, IIT Bombay India

NCFMFP2006-1221

EFFECT OF COMPRESSIBILITY CORRECTIONS TO TURBULENCE MODELS APPLIED TO A HYPERSONIC RE-ENTRY CONFIGURATION

Kushal S. Kedia
Department of Aerospace Engineering
Indian Institute of Technology Madras
Chennai, India.

Krishnendu Sinha *
Department of Aerospace Engineering
Indian Institute of Technology Bombay
Mumbai, India.

ABSTRACT

Computation of high-speed turbulent flows using conventional turbulence models developed for incompressible flows can lead to significant errors. This is especially true for high-speed vehicles where the Mach number ranges from low subsonic at the nose to hypersonic values along the body. The flow field is further complicated by boundary layer transition on fore-body, flow separation behind the vehicle, and turbulent free shear layer recompression in the reattachment region. Several compressibility corrections to conventional turbulence models have been proposed to account for these high Mach number effects. This paper evaluates such modifications to one- and two-equation turbulence models. The test case considered is the flow around a hypersonic re-entry configuration with a large recirculation region behind the vehicle. Issues pertaining to the implementation of the models and their modifications to a practical configuration are discussed. The effect of the different models and compressibility corrections are studied in terms of the predicted boundary layer transition location, size of the recirculation region, and the resulting pressure and heat transfer rate on the vehicle.

NOMENCLATURE

a	speed of sound, ms^{-1}
M	Mach number
M_c	Convective Mach number
ν	kinematic molecular viscosity, $\mathrm{m}^2\mathrm{s}^{-1}$
ν_T	kinematic eddy viscosity, $\mathrm{m}^2\mathrm{s}^{-1}$
$\bar{\rho}$	mean density, $\mathrm{kg/m}^3$
q	heat transfer rate per unit area, $\mathrm{Watt/cm}^2$
p	pressure, Pa
s	body co-ordinate, m
D	body diameter, m
U	velocity, ms^{-1}
Ω	magnitude of mean vorticity vector, s^{-1}
k	turbulent kinetic energy
ε	turbulent kinetic energy dissipation rate
ω	specific dissipation

INTRODUCTION

Atmospheric re-entry vehicles are subjected to large aerothermal loads. During the later part of their descent the flow around the vehicle, especially in the wake region, may transition to turbulence. This can significantly increase the heat transfer to the vehicle walls. Predicting the turbulent heating rate is challenging, and the inaccuracies are generally compensated by a large safety factor in the design of heat shields [1].

Engineering prediction of turbulent flows relies mostly on Reynolds-averaged Navier Stokes (RANS) simulations that compute the time-averaged flow field. Turbulence closure is obtained using RANS turbulence models which were originally developed for incompressible flows. As noted by Paciorri in [22], fluid compressibility adds to turbulence phenomenology new specific processes and mechanisms, such as new pathways for energy ex-

*Address all correspondence to this author (krish@aero.iitb.ac.in).

changes, and strong coupling between momentum and energy exchanges. This can significantly alter the turbulent characteristics and the flow behavior. A detailed review of compressibility and its effects on turbulence can be found in [2]. Compressibility effects play an important role in turbulent mixing layers. Numerous studies [3], [4], [5] have highlighted that the spreading rate of a mixing layer is reduced with respect to an analogous incompressible mixing layer.

Many research groups are working on methods of including these compressibility effects in conventional turbulence models to predict more realistic flow-fields for compressible conditions. Catris and Aupoix [21], Paciorri and Sabetta [22], Secundov et al [25], and Spalart [24] have shown various compressibility modifications to existing turbulence models to predict the effects of compressibility on shear layers and other aspects of a flow-field. Compressibility corrections have also been proposed by Sarkar et al [29] and Zeman [30]. Majority of these modifications aim to achieve the reduced spreading rate of free shear layer at high Mach numbers.

For bluff bodies, flows are complex in nature [6] because they involve interaction of a wake, separated flow, free shear layer, and boundary layer. Brown [18] recently computed the flow around a re-entry configuration where the flow transitions on the afterbody and the sting. The compressibility corrected SST model was found most accurate. Brown also highlights the consistency and accuracy of numerous turbulence models, with and without compressibility corrections, in predicting heat transfer levels for a range of hypersonic flows. Sinha [12] computed the flow-field around Fire II re-entry configuration using standard $k-\omega$ and SA turbulence models. Large differences between the turbulence model predictions are found in the vicinity of the transition location on the forebody. Variation of separation bubble size and afterbody pressure and heat transfer as obtained by the two turbulence models are also highlighted.

Transition from laminar to turbulent in high speed boundary layers is important for prediction and control of heat transfer, skin friction, etc. A lot of research is directed towards predicting correctly this transition in high speed flows. A large number of parameters influence this transition such as Mach number, transverse and streamwise curvature, pressure gradient, temperature, and cross flow [7]. A survey of flight data for boundary layer transition at hypersonic speeds is done by Schneider [8]. Lees [14] highlights the laminar-turbulent transition in hypersonic wakes and summarizes crisply the effect of Reynolds number in transition.

Similar to simulations done by Sinha in [12], the current paper studies the transitional/turbulent flow along the Fire II vehicle using RANS turbulence models. Compressibility corrections are included in turbulence models to understand the effect of these corrections in predicting realistic flowfield around a re-entering vehicle. Although the temperature in the flowfield is high enough for the chemical reactions to occur, the current simulations assume perfect gas and effect of thermo-chemistry is neglected. This is because of the focus of the study is to understand the behavior of turbulence models and compressibility corrections to them at low Reynolds number and high Mach number conditions, typical of re-entry conditions.

1 SIMULATION METHODOLOGY AND TEST CASE

The grid topology, freestream conditions, boundary conditions and computational approach is the same as described by Sinha in [12]. The Fire II vehicle has a spherical forebody and a conical afterbody [19]. The vehicle dimensions are shown in Fig. 1. The simulations in [12] correspond to an altitude of 35 km, where the freestream density and temperature are 0.0082kg/m^3 and 237 K respectively. The vehicle velocity is 5 km/s (Mach 16) at zero angle of attack. The wall temperature is 553.3 K and the Reynolds number based on freestream flow and vehicle diameter is 1.76×10^6. Note that a detailed grid refinement study is presented in Ref. [12] and the current simulations are run on the baseline grid for each case. The turbulence models and compressibility corrections are described below.

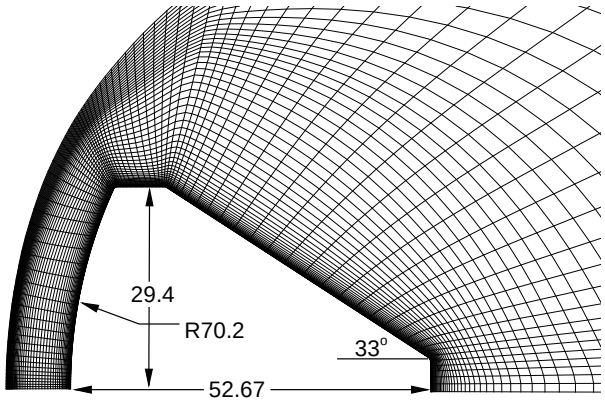

Figure 1. Computational Domain in the vicinity of the vehicle

1.1 Spalart Allmaras model (SA) and its modifications

Spalart-Allmaras (SA) one equation turbulence model [20] solves the following conservation equation for variable $\tilde{\nu}$.

$$\frac{D\bar{\rho}\tilde{\nu}}{Dt} = c_{b1}\bar{\rho}\tilde{S}\tilde{\nu} - c_{w1}f_w\bar{\rho}\left[\frac{\tilde{\nu}}{d}\right]^2 + \frac{\bar{\rho}}{\sigma}[\nabla\cdot((\nu+\tilde{\nu})\nabla\tilde{\nu}) + c_{b2}(\nabla\tilde{\nu})^2]$$

The left hand side represents the material derivative of $\bar{\rho}\tilde{\nu}$, and the terms on the right hand side correspond to production, destruction and diffusion mechanisms in the flow. The turbulent

viscosity is given by

$$\nu_t = \tilde{\nu} f_{v1}, \quad f_{v1} = \frac{\chi^3}{\chi^3 + c_{v1}^3}, \quad \chi = \frac{\tilde{\nu}}{\nu}.$$

S is the magnitude of the mean vorticity and

$$\tilde{S} = S + \frac{\tilde{\nu}}{\kappa^2 d^2} f_{v2}, \quad f_{v2} = 1 - \frac{\chi}{1 + \chi f_{v1}},$$

d is the distance to the nearest wall. The non dimensional wall destruction function is

$$f_w = g\left[\frac{1 + c_{w3}^6}{g^6 + c_{w3}^6}\right], \quad g = r + c_{w2}(r^6 - r), \quad r = \frac{\tilde{\nu}}{S\kappa^2 d^2}$$

The model constants are $c_{b1} = 0.1355$, $c_{b2} = 0.622$, $\sigma = 2/3$, $\kappa = 0.41$, $c_{w1} = 0.3$, $c_{w2} = 0.3$, and $c_{w3} = 2$.

Catris and Aupoix proposed a density correction [21] to the SA turbulence model (SA-cat) for improvement of the predictions of high Mach number boundary layers. The transported quantity remains $\tilde{\nu}$ and the diffused quantity is $\sqrt{\bar{\rho}}\tilde{\nu}$, such that the diffusion term becomes

$$\frac{1}{\sigma}[\nabla \cdot ((\bar{\rho}\tilde{\nu} + \sqrt{\bar{\rho}}\tilde{\nu})\nabla\sqrt{\bar{\rho}}\tilde{\nu}) + c_{b2}(\nabla\sqrt{\bar{\rho}}\tilde{\nu} \cdot (\nabla\sqrt{\bar{\rho}}\tilde{\nu}))]$$

The SA-cat model is compatible with the logarithmic law. The turbulent diffusion term and the cross term are independent of the density gradient in the logarithmic layer.

Paciorri and Sabetta proposed a correction [22] to the SA turbulence model (SA-pac) to account for the compressibility effects in the mixing layers which separate the low speed recirculation regions from high speed streams in supersonic afterbody flows. Unlike other corrections proposed for two-equation models, the SA-pac correction does not need the knowledge of the turbulent Mach number, and therefore is useful for one equation models like SA which do not directly integrate the turbulent kinetic energy equation. The fundamental parameter governing the compressibility effects in this model is the convective Mach number, M_c. The production term is modified to

$$f_1(M_c) f_2(M_c) c_{b1} \bar{\rho} \tilde{S} \tilde{\nu}$$

where

$$f_1(M_c) = \frac{0.6}{1 + 9M_c^6} + 0.4, \quad f_2(M_c) = \frac{0.44}{1 + 14M_c^6} + 0.56$$

Local estimate of Convective Mach number M_c is obtained by solving the following equation using Newton Raphson method.

$$M_c^2 f_2(M_c) = \frac{\nu_t S}{4\tau_i a^2}$$

where a is the speed of sound and τ_i dimensionless shear stress for incompressible flow as defined in [22]. The value of $\tau_i = 0.01$. The right hand side of the above equation is a function of vorticity which defines the convective Mach number.

Multiplying the production term by a factor $f_1(M_c) f_2(M_c)$ reduces eddy viscosity thereby reducing the growth rate of free shear layer as observed experimentally for compressible flows. Correction is applied only in the free shear layer since it deteriorates the behavior of SA model in boundary layers. The free shear layer is approximated as the region with $M_c > 1$. Region with $M_c > 1$ can be mathematically identified by

$$\frac{\nu_t S}{4\tau_i a^2} > 0.65$$

Secundov et al proposed a compressibility correction [25] to the SA turbulence model (SA-sec) to account for the reduced growth rate of compressible shear layers. The closure equation for SA-sec model has the following additional term ($C_5 = 3.5$).

$$-\frac{C_5 \tilde{\nu}^2 \nabla U \nabla U}{a^2}$$

This additional term accounts for the reduction in spreading rate of the compressible shear layer by reducing the turbulent eddy viscosity ν_t as observed experimentally. Correction is applied for two cases, throughout the afterbody (SA-sec1) and only in the free shear layer (SA-sec2). The free shear layer is approximated as the region with $M_c > 1$.

1.2 Wilcox's k - ω model (kw)

The 1988 version of Wilcox [28] $k-\omega$ turbulence model is:

$$\frac{D\bar{\rho}k}{Dt} = P_k - \beta_k \bar{\rho} k\omega + \nabla \cdot ((\mu + \sigma_{k1}\mu_t)\nabla k)$$
$$\frac{D\bar{\rho}\omega}{Dt} = \gamma_1 P_k(\omega/k) - \beta_1 \bar{\rho}\omega^2 + \nabla \cdot ((\mu + \sigma_{\omega 1}\mu_t)\nabla\omega)$$

The left hand sides represents the material derivative of $\bar{\rho}k$ and $\bar{\rho}\omega$, and the terms on the right hand side correspond to production, destruction and diffusion mechanisms in the flow. The

turbulent kinetic energy production term is:

$$P_k = \tau_{ij}\frac{\partial u_i}{\partial x_j}$$
$$\tau_{ij} = \bar{\rho}\nu_t\Big(\frac{\partial u_i}{\partial x_j}+\frac{\partial u_j}{\partial x_i}-\frac{2}{3}\frac{\partial u_k}{\partial x_k}\delta_{ij}\Big)-\frac{2}{3}\bar{\rho}k\delta_{ij}$$

The turbulent viscosity is given by $\nu_t = k/\omega$, and the constants are $\beta_k = 0.09$, $\beta_1 = 0.075$, $\sigma_{k1} = \sigma_{\omega 1} = 0.5$ and $\gamma_1 = 0.5532$.

1.3 Shear stress transport model (sst) and its modifications

The shear stress transport(sst) turbulence model [27] is identical to the $k-\omega$ equations given above except for the following additional term in the ω-equation

$$2(1-F_1)\bar{\rho}\sigma_{\omega 2}\frac{1}{\omega}\nabla k\cdot\nabla\omega$$

The turbulent viscosity is given by

$$\nu_t = k/\max(\omega, \Omega F_2/a_1)$$

The constants ϕ of the new model are calculated from the constants ϕ_1, ϕ_2 as follows:

$$\phi = F_1\phi_1 + (1-F_1)\phi_2$$

The first set (ϕ_1) correspond to the $k-\omega$ model: $\beta_k = 0.09$, $\beta_1 = 0.075$, $\sigma_{k1} = 0.85$, $\sigma_{\omega 1} = 0.5$ and $\gamma_1 = 0.5532$. The second set (ϕ_2) are for the standard $k-\varepsilon$ model: $\beta_k = 0.09$, $\beta_2 = 0.0828$, $\sigma_{k2} = 1.0$, $\sigma_{\omega 2} = 0.856$ and $\gamma_2 = 0.44$. The blending functions F_1 and F_2 are defined as follows:

$$F_1 = tanh(arg_1^4)$$
$$arg_1 = \min\left[\max\Big(\frac{2\sqrt{k}}{0.09\omega y}, \frac{500\nu}{y^2\omega}\Big), \frac{4\bar{\rho}\sigma_{\omega 2}k}{CD_{k\omega}y^2}\right]$$
$$CD_{k\omega} = \max\Big(2\bar{\rho}\sigma_{\omega 2}\frac{1}{\omega}\frac{\partial k}{\partial x_j}\frac{\partial \omega}{\partial x_j}, 10^{-20}\Big)$$
$$F_2 = tanh(arg_2^2)$$
$$arg_2 = \max\Big(\frac{2\sqrt{k}}{0.09\omega y}, \frac{500\nu}{y^2\omega}\Big)$$

The primary compressibility effect considered here is a correction needed to account for the reduction in a free shear layer growth due to compressibility. Wilcox [28] describes a modification to the corrections of Sarkar et al. [29] and of Zeman [30] where the dissipation of k increases with turbulent Mach number, M_T, and the dissipation of ω decreases with turbulent Mach number, according to

$$D_{k,c} = D_k[1+1.5F(M_T)]$$
$$D_{\omega,c} = D_\omega[1-1.5(\beta_k/\beta_\omega)F(M_T)]$$

where,

$$F(M_T) = |M_T^2 - M_{TO}^2|, \quad \text{if} \quad M_T^2 > M_{TO}^2$$
$$= 0\text{ , otherwise}$$
$$M_T^2 = 2k/a^2, \text{ and } M_{TO} = 1/4$$

The M_{T0} term was introduced by Wilcox so these corrections would be active in compressible free shear layers, where the turbulent Mach number is high, but inactive in the near wall region of boundary layer flows where the turbulent Mach number tends to be lower. Wilcox verified the behavior of this correction to both free mixing layers and boundary layer flows up to Mach 5. In this paper, the sstc1 turbulence model is specified as being the SST turbulence model with the Wilcox compressibility correction.

As noted by Brown in [18], for turbulent boundary layers above Mach 5, the turbulent Mach number can easily exceed M_{T0}, leading to a significant reduction in skin friction and heat transfer predicted for high Mach number turbulent boundary layers when using the sstc1 turbulent model. In order to allow use of the compressibility correction for Mach number above 5, the Wilcox compressibility correction is modified by a redefinition of the turbulent Mach number to create the sstc2 turbulence model option, where:

$$F(M_T) = |M_T^2 - M_{TO}^2|, \quad \text{if} \quad M_T^2 > M_{TO}^2$$
$$= 0\text{ , otherwise}$$
$$M_T^2 = 2k(1-F_1)/a^2, \text{ and } M_{TO} = 1/4$$

The F_1 function is already defined for the sst model and has the advantage of being a logical indicator of whether the immediate region is the near wall region of a turbulent boundary layer. The result is that for the sstc2 turbulence model, the compressibility correction is applied only outside of the near wall region of a turbulent boundary layer, regardless of turbulent Mach number.

Note that the shock-unsteadiness modification [17] is used in all the two-equation model simulations. As described in [12] this is required to limit the turbulence amplification at the bow shock. Also, the f_w damping function in the SA model is modified as

per [12] to avoid unphysical heat transfer rates on the afterbody. The SA-cat model is proposed for compressibility effects in the boundary layer. Its effect on afterbody flow is also analyzed by applying the corrections throughout the forebody and afterbody. By comparison, the SA-pac, SA-sec1 and SA-sec2 models are proposed for free shear layers, and are therefore not applied on the forebody. SA-sec1 model has compressibility corrections in the full afterbody domain. The SA-pac and SA-sec2 models have compressibility corrections included only in the free shear layer. Compressibility modifications to sst models are applied throughout the domain of the forebody and afterbody.

2 SIMULATION RESULTS

Figure 2 shows a typical flowfield simulation in terms of the temperature distribution around the vehicle as computed by Sinha [12]. The free stream flow is from left to right and is slowed down by the bow shock ahead of the body. The flow on the forebody is subsonic and it becomes supersonic right before the first expansion corner at the shoulder. This is followed by a second expansion on to the conical frustum. The boundary layer separates immediately downstream of the second corner to form a shear layer that encloses a recirculation region. The shear layer encloses a toroidal vortex that extends from the shoulder to the neck region where a re-compression shock is formed to turn the supersonic flow outside the wake. The flow in the recirculation region is mostly subsonic and it expands downstream of the neck to form a supersonic wake.

The forebody pressure and heat transfer can be seen in Fig. 3. The pressure and heat transfer has a maximum at the nose(s=0) because of the stagnation point. Pressure then follows a parabolic profile on the forebody with a sharp decrease around the first expansion corner ($s/D = 0.51$). The heat transfer increases after an initial drop as the boundary layer flow transitions from laminar to turbulent. There is a sharp peak in heating rate at the expansion corner. The Reynolds number near the transition location ($s/D \sim 0.2$) is of the order of 10^4 and Mach number is around 0.3. This is significantly lower than values observed in [8], but is in agreement with the fact that transitional *Re* is greatly reduced by large nose bluntness [13] typical of reentry vehicles. Ref. [13] also mentions that for highly cool walls, there is an evidence of transitional Re decreasing considerably. The forebody wall is highly cooled in the current simulations ($T_w/T_{aw} = 0.05$).

2.1 One-equation turbulence models

The Catris-Aupoix compressibility correction to the SA model doesn't reflect much of a difference in the surface pressure and heat transfer results of the present body. Even the velocity profiles in the log layer show negligible change. Catris [21] points out that difference between the SA model and the modified SA-cat model decreases when the wall temperature to adiabatic wall temperature ratio decreases, since density gradient effect is less important. In the present case, this temperature ratio is about 0.05 on the forebody and about 0.3 on the afterbody. Also Catris [21] explains that the density corrections act upon the mean velocity profile through the eddy viscosity level. So they vanish near the wall because of the damping function and at the edge of the boundary layer with density gradient.

Fig. 4 shows a comparison of temperature flowfield using SA-pac and SA models. A few representative streamlines are also shown. The size of the separation bubble is larger in the

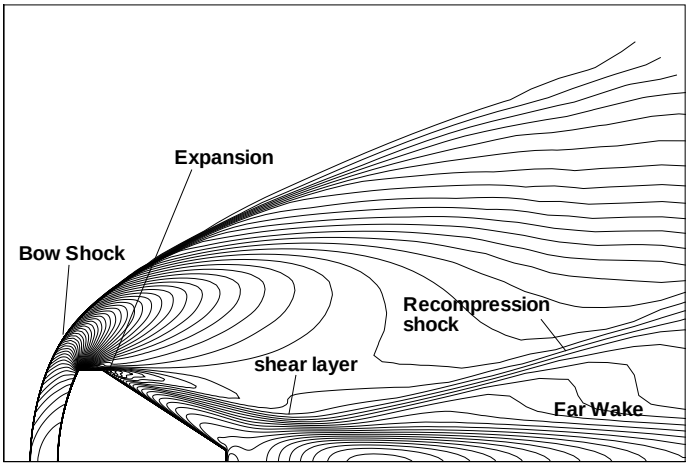

Figure 2. Computed temperature field around the Fire II vehicle. The key flow features are identified.

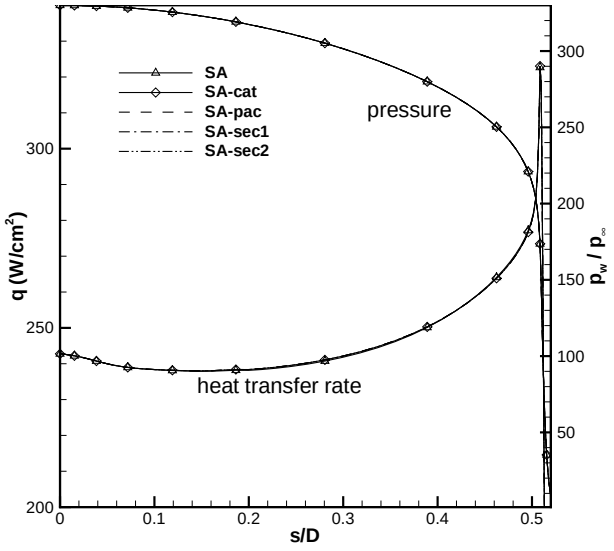

Figure 3. Heat transfer rate and normalized pressure on the forebody computed using the SA model.

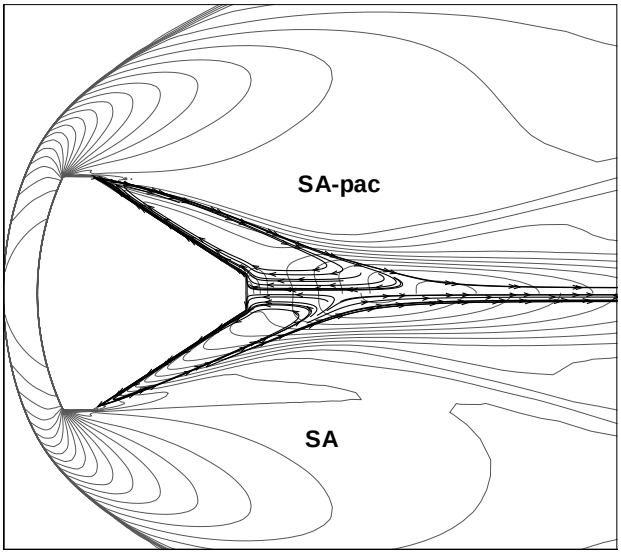

Figure 4. Comparison of temperature contours and representative streamlines in the separation bubbles computed using the SA and SA-pac models.

SA-pac solution than that in the SA solution. This is because the eddy viscosity predicted in the SA-pac model is lower in the wake as compared to SA model. The production term is multiplied by a reducing factor of $f_1(\mathrm{M}_c)f_2(\mathrm{M}_c)$ to account for the reduced shear layer spreading rate at high convective Mach number. Lower eddy viscosity leads to lower temperature in the wake of SA-pac solution. Similar trend can be seen when the SA-sec1 and SA-sec2 solutions are compared with SA solution. The eddy viscosity in the SA-sec afterbody solution is less because of the additional destruction term due to compressibility effects.

The disparity in the size of the recirculation regions leads to difference in the afterbody wall pressure (Fig. 5). Smaller recirculation region results in larger flow expansion around the vehicle shoulder leading to lower pressure on the afterbody for SA solution as compared to other solutions. Even the base pressure predicted by SA solution is less than the other solutions, as observed by Forsythe et al [26] and Paciorri [22]. Note that pressure obtained using SA-cat is identical to the SA model. Fig. 5 also shows the effect of the compressibility correction on the afterbody wall heat transfer. The heating rates obtained using the SA and SA-cat models are almost identical except at the base. SA-pac and SA-sec2 predictions are comparable to the SA values along majority of the afterbody. However, near the separation point and in the region just before the base, the heat transfer rate differs considerably. The SA-sec2 and SA-pac solutions underpredict heat transfer as compared to the SA solution. The base heat transfer rate is higher for these models than the SA solution.

For SA-sec1 solution, there are large fluctuations in the heat transfer rate, which move back and forth along the afterbody, so

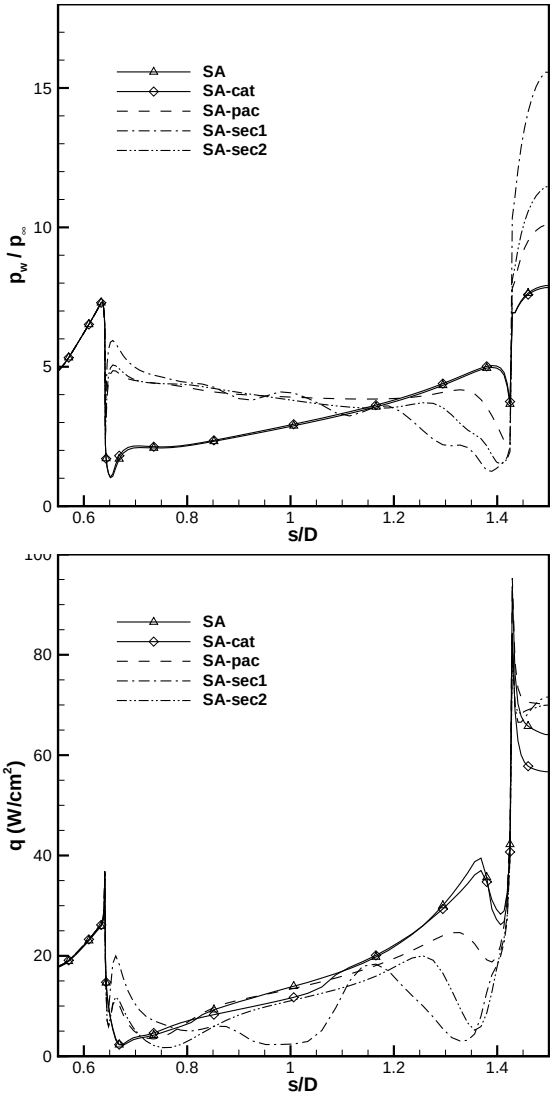

Figure 5. Comparison of normalized pressure and heat transfer on the afterbody computed using SA model and its variants.

that a steady state solution cannot be obtained in this case. These heating rate fluctuations correspond to secondary separation in the afterbody recirculation bubble, as can be seen in Fig. 6. This is in contrast to the other model solutions which result in a single toroidal vortex spanning the entire recirculation region. Fig. 7 shows a typical variation of normalized turbulent eddy viscosity across the recirculation bubble at a certain location on the conical frustum. The application of the compressibility correction in the entire afterbody flowfield (SA-sec1) results in very low values of the turbulent eddy viscosity. The flow in the recirculation bubble is essentially laminar in this case. Also, when carefully observed, a shock can be seen in the SA-sec1 solution just after the base Fig.8. This is probably because of a large separation bubble. The

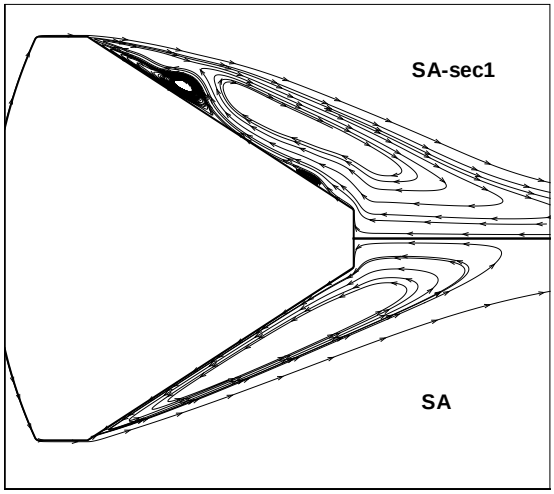

Figure 6. Streamlines in the SA-sec1 solution showing multiple vortices near the wall.

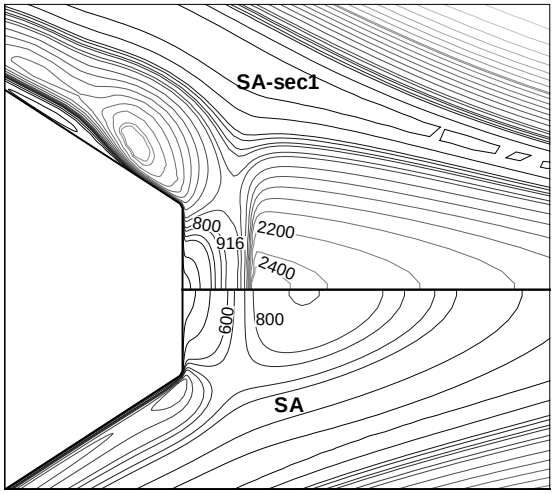

Figure 8. Velocity contours obtained using the SA-sec1 and SA models. Shock can be seen in the SA-sec1 solution. Few typical values are marked in SI units.

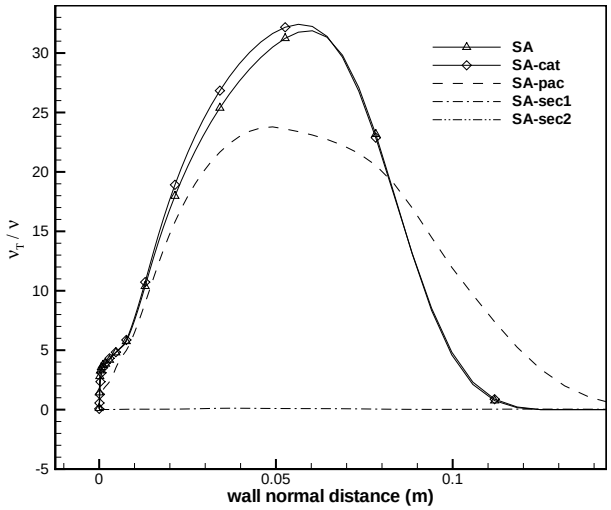

Figure 7. The ratio of turbulent eddy viscosity to kinematic viscosity at a certain location inside the separation bubble.

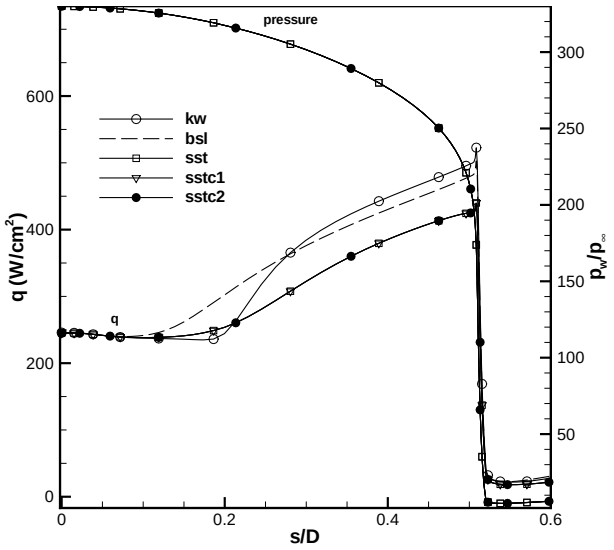

Figure 9. Comparison of Heat transfer rate and normalized wall pressure on the forebody as predicted by the different two-equation models.

flow coming towards the base accelerates to supersonic speeds due to large separation bubble and thus have to undergo a shock to meet stagnation conditions at the base. Due to this shock, the pressure value is quite high at the base as observed in Fig. 5.

2.2 Two-equation turbulence models

The normalized wall pressure and heat transfer rate obtained using the kw, bsl, sst, sstc1 and sstc2 turbulence closure models on the forebody can be seen in Fig. 9. The wall pressures predicted by all the models overlap and are identical to that obtained using the one-equation models. The heat transfer rates are however significantly different as pointed out in [12]. The heating rate shows a sharper increase at transition than the one-equation models. Among the two-equation models, bsl predicts transition upstream of kw and sst models. However, the heating rate rises more rapidly in the kw case and results in the highest peak heating at the expansion corner. Compressibility corrected sstc1 and sstc2 turbulence models predict identical pressure and heat transfer on the forebody as predicted by sst model since the turbulent Mach number in this region is small. Also the compressibility corrections were proposed in such a way that they are active only in the compressible free shear layer.

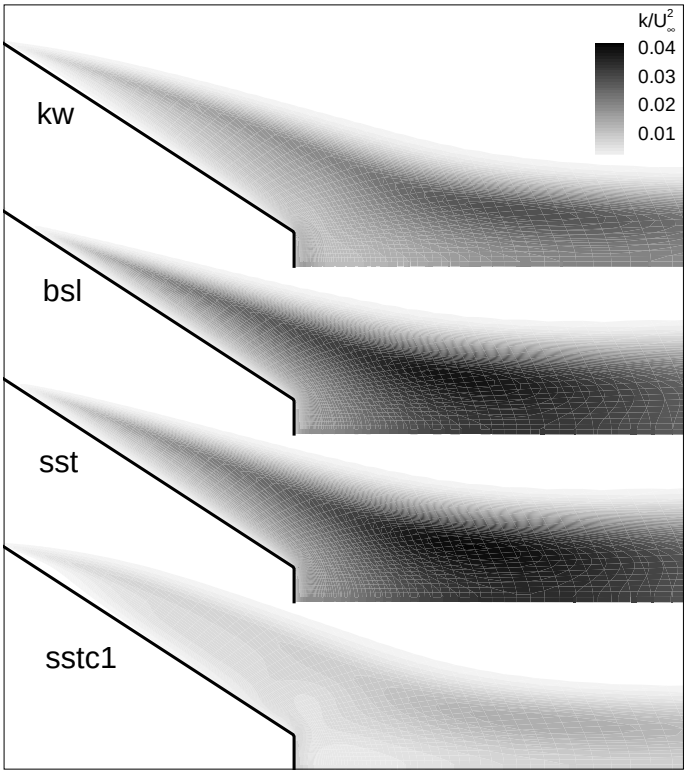

Figure 10. Contours of normalized turbulent kinetic energy as obtained using the different two-equation models.

Fig. 10 shows the normalized turbulent kinetic energy distribution in the different solutions. The $k-\varepsilon$ part of bsl model (outside boundary layer) predicts higher turbulence than the kw model. The k levels in bsl and sst solutions are comparable, whereas the compressibility corrections reduce the turbulent intensity significantly. The sstc2 results are almost identical to the sstc1 case and therefore not shown here. The location of the shear layer and the size of the recirculation region can also be identified in Fig. 10. Higher turbulence level leads to larger dissipation in the wake and therefore a smaller separation bubble. Thus, bsl predicts the smallest bubble and sstc1/c2 yield the largest size.

Afterbody surface pressure and heat transfer rates obtained using the different two-equation models and their variants are shown in Fig. 11. Smaller recirculation region leads to lower afterbody wall pressure, as can be seen by comparing the kw, sst and bsl solutions (Fig. 11). A smaller recirculation region also results in a larger variation of pressure along the afterbody frustum. The base pressure is nearly the same for these three models. The sstc1 and sstc2 models yield a different variation of pressure on the afterbody as compared to the other models, and also predict a much higher base pressure. This is because of the base shock generated in the compressibility corrected model (see Fig. 12) that is similar to the SA-sec1 solution. The afterbody

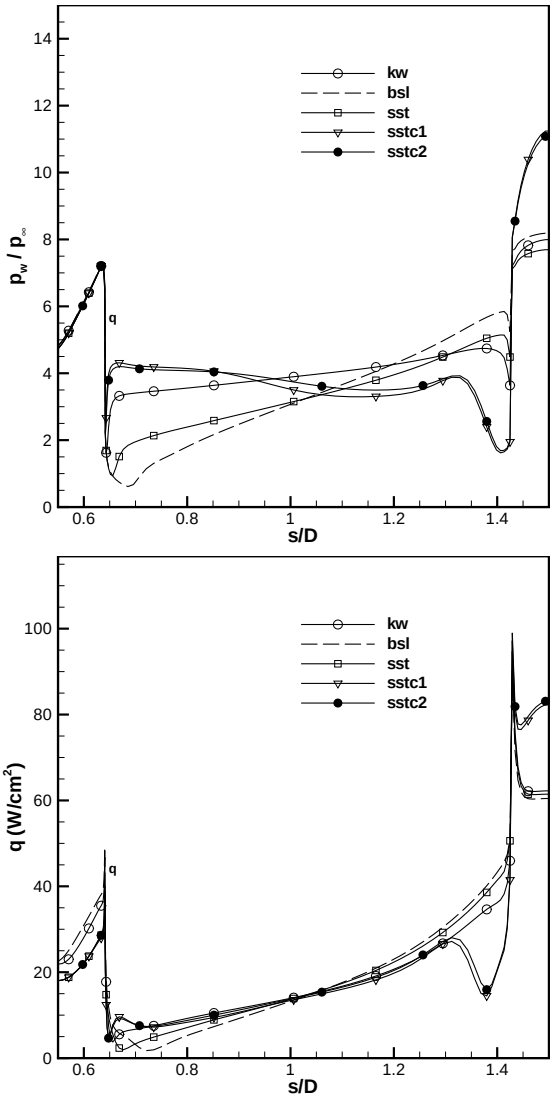

Figure 11. Comparison of afterbody normalized wall pressure and heat transfer rate predicted by the different two-equation model and their variants.

heat transfer rate predicted by the various models are nearly the same over majority of the afterbody. However, sstc1 and sstc2 models predict higher heat transfer at the base as compared to sst solution. This is also because of the shock wave at the base. Just before the second expansion corner, sstc1 and sstc2 models predict slightly lower heat transfer rates compared to the kw, bsl and sst models.

3 CONCLUSIONS

Reynolds-averaged Navier Stokes (RANS) method along with SA, $k-\omega$, and SST turbulence models are used to simu-

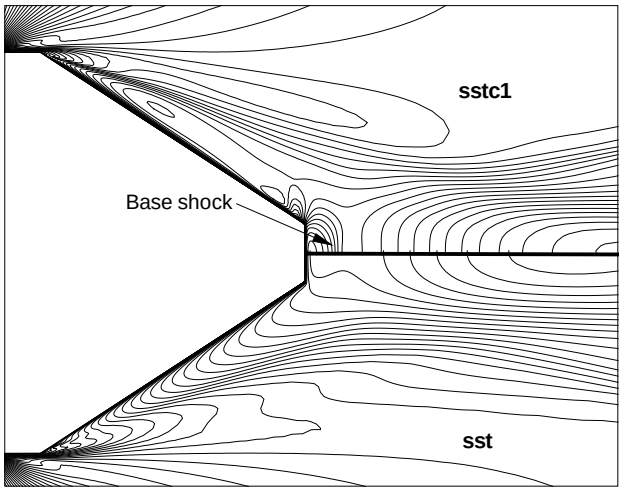

Figure 12. Comparison of temperature distribution obtained using the SST and sstc1 turbulence models.

late the FIRE II re-entry flowfield. Compressibility corrections are introduced in the SA and SST models, and their effects are assessed by comparing the respective solutions. Specifically, the afterbody pressure and heat transfer rates, and the size of the separation bubble are used for comparison. The Catris-Aupoix modification to the SA model does not alter the solution because of the fact that the ratio of wall temperature to adiabatic value is very small. The base pressure is found to increase with introduction of the other compressibility corrections due to the decrease in turbulence level and the accompanied increase in the size of separation bubble. In some compressibility corrected cases (SA-sec1 and SA-sec2) the turbulent eddy viscosity is lower than molecular viscosity, resulting in laminar solution. These flows are characterized by secondary separation and large fluctuations in the heating rates. A normal shock at the base is obtained using the compressibility corrections that results in high pressure, temperature and heating rate at the base.

REFERENCES

[1] Wright, M.J., Loomis, M.,Papadopoulos, P., "Aerothermal Analysis of Project FIRE II afterbody flow," *Journal of Thermophysics and Heat Transfer*, Vol. 17(2), 2003, pp. 60-67.

[2] Lele, S.K., "Compressibility effects on Turbulence," *Annual Review of Fluid Mechanics*, Vol. 26, 1994, pp. 211-254.

[3] Roshko, A., Papamoschou, D., "The Compressible Turbulent Shear Layer, an Experimental Study," *Journal of Fluid Mechanics*, Vol. 197, Dec. 1988, pp. 453-477.

[4] Samimy, M., Elliot, G.S., "Effects of Compressibility on the Characteristics of Free Shear Layers," *AIAA Journal* , Vol. 28, No. 3, 1990, pp. 439-445.

[5] Goebel, S.G., Dutton, J.C., "Experimental Study of Compressible Turbulent Mixing Layers," *AIAA Journal*, Vol. 29, No. 4, 1991, pp. 538-546.

[6] Roshko, A.F., "Perspectives on Bluff Body Aerodynamics," *Journal of Wind Engineering and Industrial Aerodynamics*, Vol. 49, 1993, pp. 79-100.

[7] Reshotko, E., "Boundary Layer Instability, Transition and Control," AIAA Paper 94-0001, Jan 1994.

[8] Schneider, S. P., "Flight Data for Boundary Layer Transition at Hypersonic and Supersonic Speeds," *Journal of Spacecrafts and Rockets*, Vol. 36, No. 1, Jan 1999.

[9] Dhawan, S., Narsimha, R., "Some properties of boundary layer flow during the transition from laminar to turbulent motion," *Journal of Fluid Mechanics*, Vol. 3, No. 4, 1958, pp. 418-436.

[10] Nance, R.P., Horvath,T.J., Hassan, H.A., "Transition and Turbulence Modelling for Blunt-Body Wake Flows," AIAA paper 97-2570, 1997.

[11] Robinson, D.F., Harris, J.E., Hassan, H.A., "Unified Turbulence Closure model for Wall bounded and Free Shear Flows," *AIAA Journal*, Vol. 33, No. 12, Dec. 1995, pp. 2325-2331.

[12] Sinha, K., "Reynolds-averaged Navier-Stokes simulation of Fire II re-entry configuration," 25th International Symposium on Shock Waves ISSW25, Jul 2005.

[13] Anderson, J., "Viscous Flow: Basic Aspects, Boundary Layer Results and Aerodynamic Heating," *Hypersonic and High Temperature Gas Dynamics*, AIAA, pp. 271-300.

[14] Lees, L., "Hypersonic Wakes and Trails," *AIAA Journal*, Vol. 2, No. 3, March 1964, pp. 417-428.

[15] Sinha, K., Candler, G.V., "An Accurate Implicit Formulation of a Two Equation Turbulence Model," AIAA paper 98-2649, 1998.

[16] Sinha, K., Mahesh, K., Candler, G.V., "Modelling Shock Unsteadiness in Shock/Turbulence Interaction," *Physics of Fluids*, Vol. 15., No. 8, 2003, pp. 2290-2297.

[17] Sinha, K., Mahesh, K., Candler, G.V., "Modelling the Effect of Shock Unsteadiness in Shock-Wave/Turbulent Boundary Layer Interactions," *AIAA Journal*, Vol. 15., No. 8, 2003, pp. 2290-2297.

[18] Brown, J.L., "Turbulence Model Validation for Hypersonic Flows," AIAA 2002-3308, June 2002.

[19] Sloucomb, T.H. ,"Project Fire II afterbody temperature and pressure at 11.35 km per second," NASA TM X-1319, 1966.

[20] Spalart, P.R., Allmaras, S.R., "A one-equation Turbulence Model for Aerodynamic Flows," 30th AIAA Aerospace Sciences Meeting and Exhibit, AIAA 92-0439, Jan 1992.

[21] Catris, S., and Aupoix, B., "Density Corrections for Turbulence Models," *Aerospace Science and Technology*, Vol. 4, 2000, pp. 1-11.

[22] Paciorri, R., and Sabetta, F., "Compressibility Correction for the Spalart-Allmaras Model in Free-Shear Flows," *Journal of Spacecraft and Rockets*, Vol. 40, No. 3, 2003, pp. 326-

331.

[23] Paciorri, R., and Sabetta, F., Nasuti, F., "Evaluation of Turbulence modelling in supersonic afterbody Computations," AIAA Fluid Dynamics Conference and Exhibit, AIAA 2001-3039, June 2001.

[24] Spalart, P. R., "Trends in Turbulence Treatments," AIAA 00-2306, July 2000.

[25] Shur, M., Strelets, M., Zaikov, L., Gulyaev, A., Kozlov,V., and Secundov, A., "Comparative Numerical Testing of One- and Two- Equation Turbulence Models for Flows with Separation and Reattachment," AIAA 95-0863.

[26] Forsythe, J.R., Hoffmann, K.A., Squires, K.D., "Detached-Eddy Simulation with Compressibility Corrections Applied to a Supersonic Axisymmetric Base Flow," 40th AIAA Aerospace Sciences Meeting and Exhibit, AIAA 02-0586, Jan 2002.

[27] Menter, F.R., "Two-Equation Eddy-Viscosity Turbulence Models for Engineering Applications," *AIAA Journal*, Vol. 32, No. 8, August 1994, pp. 1598 - 1605.

[28] Wilcox, D.C., "Turbulence Modelling for CFD," DCW Industries, Inc., 5354 Palm Drive, La Canada, CA, 2nd ed., 1998.

[29] Sarkar, S., Erlebacher, G., Hussaini, M.Y., and Kreiss, H.O., "The Analysis and Modelling of Dilatational terms in Compressible Turbulence," *Journal of Fluid Mechanics*, Vol. 227, June 1991, pp. 473-936.

[30] Zeman, O., "Dilatational Dissipation: The Concept and Application in Modelling Compressible Mixing Layers," *Physics of Fluids A*, Vol.2, No.2, Feb. 1990, pp. 178-188.